Finite element modelling of hardening concrete: application to the prediction of early age cracking for massive reinforced structures

Laurie Buffo-Lacarriere, Alain Sellier, Anaclet Turatsinze, Gilles Escadeillas

Finite element modelling of hardening concrete: application to the prediction of early age cracking for massive reinforced structures

L. Buffo-Lacarrière
Université de Toulouse, UPS, INSA, Laboratoire, Matériaux et Durabilité des Constructions (LMDC), Toulouse, France
e-mail: buffo-lacarriere@insa-toulouse.fr
VINCI Construction Grands Projets, Rueil-Malmaison, France

A. Sellier, A. Turatsinze, G. Escadeillas
Université de Toulouse, UPS, INSA, Laboratoire, Matériaux et Durabilité des Constructions (LMDC),Toulouse, France

Abstract This article presents finite element modelling to predict the early age cracking risk of concrete structures. It is a tool to help practitioners choose materials and construction techniques to reduce the risk of cracking. The proposed model uses original hydration modelling (allowing composed binder to be modelled and hydric consumption to be controlled) followed by a non-linear mechanical model of concrete at early ages involving creep and damage coupling. The article considers hydration effects on this mechanical model, which is based on a non-linear viscoelastic formulation combined with an anisotropic, regularized damage model. Details of the numerical implementation are given in the article and the model is applied successively to a laboratory structure and to a massive structure in situ (experimental wall of a nuclear power plant studied in the framework of the French national research project CEOS.fr).

Keywords Early age · Mechanical behaviour · Creep · Damage · Numerical modelling

1 Introduction

The early age cracking of structures is a serious concern in the construction industry. The occurrence of localized cracks in structures during the construction phase lead to possible aspect problems sometimes difficult to accept by structure's owners. On another hand these cracks can lead to durability problems if their opening is excessive. In this context, the purpose of the work presented here is to supply to practitioners with a numerical simulation tool able to quantify the early age cracking pattern of structures in situ. This tool can then be considered as a relevant help in the process of choosing appropriate concrete formulations and construction techniques to prevent or limit cracking.

With this aim, initial work was performed to predict the evolution of hydration in structures cast using composed binders (cement and pozzolanic additions) [10]. The physicochemical phenomena occurring as hydration develops can be causes of early age cracking. Based on a multiphasic approach, the hydration model allows several solid phases (cement and additions) to be investigated under different environmental conditions. It was built in a finite element framework to predict the hydration

evolution not only in endogenous conditions but also in real conditions, where the effects of water exchange, solar radiation and wind are properly taken into account.

The realistic prediction of hydration degrees, temperature and water content obtained with the hydration model can then be used in the early age mechanical model to assess the cracking of structures. Early age cracking of concrete structures will occur under the effect of stresses that are consequences of hydration in real environmental conditions. Many physical phenomena have to be considered in order to model the occurrence of this early age cracking:

- variation of the mechanical properties induced by binder hydration (hydration degree α predicted by the model presented in [10]
- internal strains imposed by the variations of temperature in the concrete (temperature T predicted as presented in [10]),
- damage behaviour of concrete, which governs the occurrence of cracking,
- delayed behaviour of concrete (research performed during recent decades shows that precise modelling of delayed phenomena needs to take relatively complex behaviour into consideration [1], both for autogenous behaviour and for delayed strains induced by drying. This last part is not treated in this article, which focuses on massive elements, but has been presented and validated in [27]). In fact in massive structures, the thermal strains are greater than the autogenous shrinkage, and the drying concerns only a few part of the volume, such as these two last aspects can be negligible in this context.

2 State of the art

In the aim of adapting concrete mechanical models to hardening materials, Bažant [2] has proposed the solidification theory. This uses a homogenization method based on the progressive formation of new hydrates. The hardening concrete is considered as a composite that includes aggregates, hydrated paste and non-hydrated paste, in which each component has its own rheological model with characteristics that are constant over time. The global properties of the hardening material are then managed through the variable proportions of each component. This solidification theory has been widely used since it was first put forward, with many behaviour laws [18, 20, 23].

Another, easier to use, approach considers the evolution laws for mechanical characteristics within the behaviour laws. This method is employed in several codes (CESAR-LCPC, 4C-TEMP&STRESS) but the laws used in these codes do not consider the non-linear behaviour of concrete. Nevertheless, this non-linearity could strongly influence the early age behaviour of the structure and consequently its cracking risk. That is why several authors propose early age non-linear behaviour models depending, through their parameters, on hydration [16]. They are based on incremental basic creep laws, elastoplastic laws [31] or even creep-damage coupled laws [3]. The authors demonstrate the prediction capabilities of their models from an analytical point of view. However the numerical implementation of such models in a finite element code can sometimes lead to problems, as discussed in the first part of this article where a complete procedure for the implementation of a mechanical model of hardening concrete is explained. After a general presentation of the mechanical modelling, the constitutive laws will be developed in incremental form (including creep laws) so that the model can be used for hardening materials. Moreover, the numerical implementation considers the particularity of the updating of internal variables according to the hydration development. Finally, the incremental and non-linear formulation is applied to predict, through finite element modelling, the behaviour of a "laboratory structure" and of a real reinforced massive structure at early age.

3 Modelling the behaviour of hardening concrete

In order to take account of the different creep rates of concrete subjected to deviatoric or hydrostatic pressure [1], stresses and strains are divided into these different types of stress. For each one, the instantaneous elastic module (level 0 in Fig. 1) is associated with a non-linear viscoelastic module (levels 1 and 2 in Fig. 1) based on Acker and Ulm's

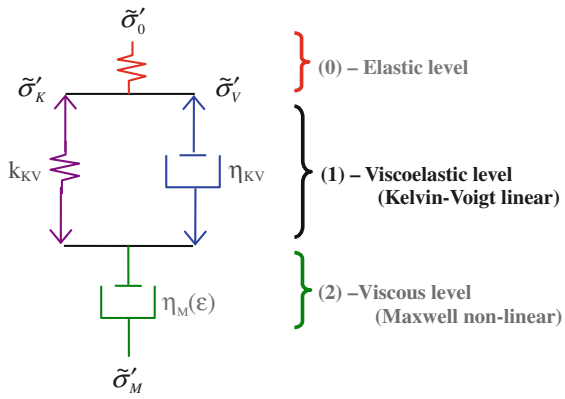

Fig. 1 Rheological model

proposals. Each level considers a particular behaviour of concrete:

- level 1, which represents paste and aggregate viscoelastic behaviour, it is responsible for the reversible part of creep,
- level 2, which models C–S–H viscous behaviour corresponds to the irreversible part resulting from sliding between C–S–H layers.

According to the damage definition of [19] and in order to take account of the connection between rheological behaviour and damage, the stress is the "effective stress" ($\tilde{\sigma}$) It is used here in an anisotropic damage model to assess the stiffness decrease due to cracking.

3.1 Constitutive laws

3.1.1 Incremental formulation of rheological laws

When concrete rheological properties are modified according to the chemical state of the material, the effective stresses are evaluated as the sum of effective stress increments observed since the start of loading (Eq. 1).

$$\tilde{\sigma} = \int_0^t \dot{\tilde{\sigma}}(\tau)\mathrm{d}\tau \tag{1}$$

The stress increment is calculated according to the corresponding strain using an adaptive differential formulation needed for chemically evolving concrete and presented in [27]. First, the total strain increment is decomposed according to the different rheological levels (Fig. 1 and Eq. 2 for the medium part):

$$\dot{\varepsilon}^{(s)} = \dot{\varepsilon}_0^{(s)} + \dot{\varepsilon}_{KV}^{(s)} + \dot{\varepsilon}_M^{(s)} + \dot{\varepsilon}_{th}^{(s)} \tag{2}$$

where $\dot{\varepsilon}^{(s)}$ is the total strain increment for the medium part, $\dot{\varepsilon}_0^{(s)}$ is the strain increment of the elastic level (level 0 in Fig. 1), $\dot{\varepsilon}_{KV}^{(s)}$ is the strain increment of the viscoelastic level (level 1 in Fig. 1), $\dot{\varepsilon}_M^{(s)}$ is the strain increment of the non-linear viscous level (level 2 in Fig. 1), $\dot{\varepsilon}_{th}^{(s)}$ is the thermal strain increment (only for volumetric change part).

It is evaluated through the temperature fields depending on a thermal model coupled with the hydration modelling.

Viscoelastic behaviour is represented by a set of constitutive relations written with effective stresses.

The equation governing the behaviour of the elastic level (0) is thus written:

$$\dot{\tilde{\sigma}}^{(s)} = k_0 \dot{\varepsilon}_0^{(s)} \tag{3}$$

where k_0 is the instantaneous elastic modulus used in level 0 of the spherical part of the stress.

At level 1, the viscoelastic behaviour of concrete is expressed by a Kelvin–Voigt model that uses laws of elasticity and viscosity in terms of stress increment:

$$\dot{\tilde{\sigma}}_{KV}^{(s)} = k_{KV}\dot{\varepsilon}_{KV}^{(s)} + \dot{\eta}_{KV}^{(s)}\dot{\varepsilon}_{KV}^{(s)} + \eta_{KV}^{(s)}\ddot{\varepsilon}_{KV}^{(s)} \tag{4}$$

where k_{KV} and $\eta_{KV}^{(s)}$ are respectively the elastic modulus and the viscosity of the Kelvin–Voigt level (level 1 in Fig. 1) of the medium part of the stress.

It should be noted that, in this relation, the viscous part has to be in a total differential form, unlike the elastic part. This is a consequence of the solidification theory: a new elastic hydration product is not subjected to the current strain since this strain state is its reference configuration, which explains the absence of a term including the variation of the elasticity coefficient multiplied by the current strain in Eq. 3. In contrast, a viscous hydration product can be immediately subjected to a strain velocity (second term in Eq. 4).

At level 2, the viscosity law is also written, for the above reasons, in terms of stress increment:

$$\dot{\tilde{\sigma}}_M^{(s)} = \dot{\eta}_M^{(s)}\dot{\varepsilon}_M^{(s)} + \eta_M^{(s)}\ddot{\varepsilon}_M^{(s)} \tag{5}$$

where $\eta_M^{(s)}$ is the viscosity of the Maxwell level of the medium part of the stress.

The compatibility between the stress increments introduced in Eqs. 2–4 finally leads to the following system:

$$\begin{cases} k_0\dot{\varepsilon}_0^{(s)} = \dot{\eta}_M^{(s)}\dot{\varepsilon}_M^{(s)} + \eta_M^{(s)}\ddot{\varepsilon}_M^{(s)} \\ \dot{\eta}_M^{(s)}\dot{\varepsilon}_M^{(s)} + \eta_M^{(s)}\ddot{\varepsilon}_M^{(s)} = k_{KV}\dot{\varepsilon}_{KV}^{(s)} + \dot{\eta}_{KV}^{(s)}\dot{\varepsilon}_{KV}^{(s)} + \eta_{KV}^{(s)}\ddot{\varepsilon}_{KV}^{(s)} \\ \dot{\varepsilon}^{(s)} = \dot{\varepsilon}_0^{(s)} + \dot{\varepsilon}_{KV}^{(s)} + \dot{\varepsilon}_M^{(s)} + \dot{\varepsilon}_{th}^{(s)} \end{cases} \tag{6}$$

For the deviatoric part of the stress, the same development is made, replacing (s) by (d) and k by μ (except for thermal strain of course, where $\dot{\varepsilon}_{th}^{(d)} = 0$).

3.1.2 Non-linear creep modelling

The specificity of rheological modelling is that it takes account of progressive C–S–H gel consolidation due to the creep strain. This consolidation is used as an amplification factor of the model's viscosities which enables the long-term strain–time shape curve observed by Brooks [8] to be reproduced.

Moreover, the consolidation corresponds to an understandable phenomenon: Under the hydrostatic pressure part of the stress, the C–S–H layers come closer together during settling and, consequently, the viscous forces due to water micro-transfers and the cohesion forces are increased, leading to the macroscopic viscosity increase [27]. As the same C–S–H are also responsible for the deviatoric phenomena, the shear viscosity is also affected. Another cause of the non-linearity observed is the strain hardening, which corresponds to the progressive hampering of strain by rigid inclusions like aggregates and crystallized hydrates.

The viscosity of the Maxwell stage (Eq. 7) is thus modified by the consolidation function Cc depending on the strain of the level under consideration (Eqs. 8, 9) [27].

$$\eta_M^{(s,d)} = \eta_m^{(s,d)0} \cdot Cc \tag{7}$$

The consolidation coefficient is chosen as an exponential function to be compatible with the long-term creep observed by Brooks [8]:

$$Cc = \frac{\eta_M^{(S)}}{\eta_M^{(s)0}} = \frac{\eta_M^{(D)}}{\eta_M^{(d)0}} = \exp\left(\frac{\left|\varepsilon_M^{(s)}\right|}{\varepsilon_M^{k}}\right) \tag{8}$$

where $\varepsilon_M^{(s)}$ is the strain of the Maxwell module (level 3 in Fig. 1) associated with the hydrostatic pressure. $\varepsilon_M^{(s,d)k}$ is a characteristic strain that manages the consolidation speed.

This modelling of consolidation leads to a permanent decrease of the creep speed under the effect of a medium load.

Note that, according to previous works [9], the consolidation coefficient must be updated according to the hydration development using the following equation, which has the consequence that new hydration products appear without consolidation, thus leading to a decrease in the averaged coefficient of consolidation on the hardened phase.

$$\frac{\partial(Cc)}{\partial\alpha} = -\frac{Cc}{\alpha} \tag{9}$$

3.1.3 Damage modelling

The anisotropic damage modelling used in this work was initially developed by Sellier [26] and recently adapted to justify the thermodynamic validity of the proposed approach. Before introducing the damage variables and associated criteria, several definitions need to be recalled.

The effective stress used in the damage model is evaluated as the sum of the effective stress coming from the rheological model (integration of $\dot{\tilde{\sigma}}$ over the time step). This formulation is restricted to unsaturated concrete here. The effective stress is split into tensile and compressive stresses so as to reproduce the different behaviour of concrete under tension and compression (Eq. 10).

$$\overline{\overline{\tilde{\sigma}}} = (\tilde{\sigma}_i^c + \tilde{\sigma}_i^t) \cdot (\vec{e}_i \otimes \vec{e}_i) \tag{10}$$

where $\tilde{\sigma}_i^c = (\tilde{\sigma}_i - |\tilde{\sigma}_i|)/2$, $\tilde{\sigma}_i^t = (\tilde{\sigma}_i + |\tilde{\sigma}_i|)/2$ and $\vec{e}_i$ is a principal direction.

Each part of the stress (compressive and tensile parts) is then used to calculate the elastic strain (Eq. 11) and the damage variable (Eq. 12) needed to evaluate the apparent stress.

The tensile and compressive elastic strains are then defined by Eq. 11.

$$\varepsilon_{ij}^{er} = \frac{1+\upsilon^0}{E^0}\tilde{\sigma}_{ij}^r - \frac{\upsilon^0}{E^0} tr(\tilde{\sigma}^r) \cdot \delta_{ij} \tag{11}$$

where: r = c for compression and r = t for tension, E^0 and υ^0 are the elastic modulus of the sound material.

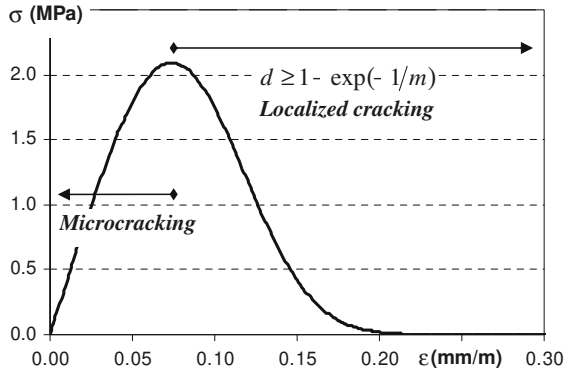

Fig. 2 Tensile behaviour law of concrete

The damage model is based on a damage variable (second order tensor in traction, in order to take account of the concrete anisotropy, and scalar in compression) which represents the cracking density in an elementary volume of material [19]. The evolution law for the damage is inspired by the Weibull law [26] classically used to describe the effects of defects in brittle materials [14]. For a principal direction i, Eq. 12 is obtained and leads to a behaviour law of the form presented in Fig. 2.

$$d_i^{\mathrm{r}} = 1 - \exp\left(-\frac{1}{m^{\mathrm{r}}}\left(\frac{\bar{\sigma}_i^{\mathrm{r}}}{\tilde{\sigma}_{\mathrm{u}}^{\mathrm{r}}}\right)^{m^{\mathrm{r}}}\right) \tag{12}$$

where: r = t (tension) or c (compression), $\bar{\sigma}_i^{\mathrm{r}}$ is the equivalent stress that characterizes the material stress history. It is evaluated with failure criteria according to the sign of the main stresses. For tensile damage, the Rankine criterion is used while, for compressive damage, it is the Drucker–Pragger criterion, expressed with the effective stresses. m^{r} and $\tilde{\sigma}_{\mathrm{u}}^{\mathrm{r}}$ are material parameters fitted using uniaxial compressive and tensile tests.

Note that, according to [9], and for the same reasons as mentioned to justify Eq. 9, the damage variable must be updated according to the hydration development using the following equation.

$$\frac{\partial D}{\partial \alpha} = -\frac{D}{\alpha} \tag{13}$$

The apparent stresses are deduced from the elastic strains and damage variables as indicated in the following paragraphs.

As the tensile damage variable is tensorial, the tensile behaviour law $\sigma^{\mathrm{t}}(\varepsilon^{\mathrm{et}})$ is written in different ways for the normal stresses and for the shear stresses.

In the main directions of the tensile damage tensor, the normal stresses are expressed as:

$$\sigma_{\mathrm{ii}}^{\mathrm{t}} = \frac{(1-d^{\mathrm{c}})E^0}{D^{\mathrm{n}}}\left[\left(\frac{1}{(1-d_i^{\mathrm{t}})(1-d_j^{\mathrm{t}})} - \upsilon^{02}\right)\varepsilon_{ii}^{\mathrm{et}} + \left(\upsilon^{02} + \frac{\upsilon^0}{1-d_i^{\mathrm{t}}}\right)\varepsilon_{jj}^{\mathrm{et}} + \left(\upsilon^{02} + \frac{\upsilon^0}{1-d_i^{\mathrm{t}}}\right)\varepsilon_{kk}^{\mathrm{et}}\right] \tag{14}$$

where:

$$D^{\mathrm{n}} = \frac{1}{(1-d_i^{\mathrm{t}})(1-d_j^{\mathrm{t}})(1-d_k^{\mathrm{t}})} - \upsilon^{02}\left(\frac{1}{1-d_i^{\mathrm{t}}} + \frac{1}{1-d_j^{\mathrm{t}}} + \frac{1}{1-d_k^{\mathrm{t}}} + 2\upsilon^0\right) \tag{15}$$

For tangential stresses, the behaviour law is written as follows:

$$\sigma_{ij}^{\mathrm{t}} = \mu^0 \varepsilon_{ij}^{\mathrm{et}} \cdot (1-d^{\mathrm{c}})(1-\max(d_i^{\mathrm{t}}, d_j^{\mathrm{t}})) \tag{16}$$

For each stress, the damage variable d^{c} is introduced in tensile behaviour law in order to generate an effect of the compressive damage on the tensile stresses.

The compressive damage is applied globally to the behaviour law because of its isotropy. The apparent stresses are written:

$$\sigma_{ij}^{\mathrm{c}} = (1-d^{\mathrm{c}})\left[\lambda^0 \cdot tr(\varepsilon^{\mathrm{ec}}) \cdot \delta_{ij} + 2\mu^0 \varepsilon_{ij}^{\mathrm{ec}}\right] \tag{17}$$

The total stress is obtained directly from the tensile and compressive principal stresses:

$$\overline{\overline{\sigma}} = \overline{\overline{\sigma}}^{\mathrm{c}} + \overline{\overline{\sigma}}^{\mathrm{t}} \tag{18}$$

The behaviour law presented in Eqs. 17, 18 reproduces the different behaviour of concrete under tension and compression and the rigidity restitution observed on a compressive test performed on a concrete previously damaged in tension. These properties are illustrated with a cyclic loading test in Fig. 3.

The localization problem induced by the softening behaviour of concrete (observed in tension and compression in Fig. 3) is managed using a method inspired by Hillerborg [17], which modifies the post-peak part of the behaviour law in order to control dissipation. This modification is carried out by a proportional transformation of the post-peak strains.

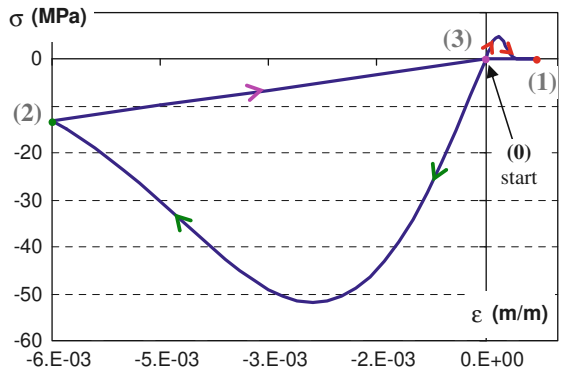

Fig. 3 Model response to a cyclic loading test

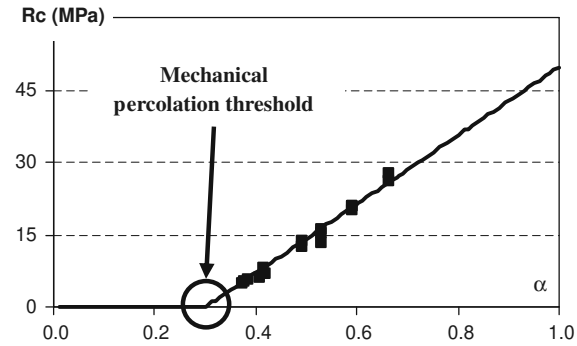

Fig. 4 Example of Young's modulus variation (for a mortar with $E/C = 0.5$)

3.2 Evolution of the mechanical properties

Recent years have seen the development of many theoretical methods able to predict the evolution of mechanical characteristics through numerical prediction of the hydration development combined with homogenization techniques [6, 25, 28, 30, 34]. Most of these models first predict the development of cement paste microstructure using microstructural models such as CEMHYD3D [5] or HYMOSTRUC [32]. Then, the concrete mechanical properties are evaluated from these paste microstructural modifications by means of homogenization techniques.

These methods have demonstrated their capacity to predict the evolution of the elastic properties of hardening concrete techniques [6, 25] but are not yet applied to predict creep characteristics and strengths. It seems difficult to apply homogenization techniques to predict a composite strength according to the strength of each phase, the major difficulty being to include the non-linearity appearing along the phase interfaces in the homogenization techniques. While waiting for progress in homogenization techniques, the development of concrete mechanical properties is modelled according to the evolution of a single averaged hydration degree (determined according to the hydration degrees of each phase of the binder).

3.2.1 Mechanical percolation threshold

In the early hours of hydration development, the concrete is subjected to strong microstructural changes. At casting time, the concrete can be consider as a fluid in which anhydrous grains and aggregate are in "suspension" in water. The transition from the fluid material to a solid that will be able to transmit an imposed deviatoric stress is made by progressive hydration of anhydrous components, which leads to the formation of a coherent material. In order to characterize the changes that cause this transition from fluid to solid, the notion of percolation threshold is introduced. This percolation threshold between solid phases corresponds to a critical hydration degree, which leads to the formation of a first percolation pathway.

To measure it, the experimental evolution of mechanical properties can be used (elastic modulus or compressive strength, see for instance Fig. 4). In this case, it is called the 'mechanical percolation threshold'. Based on a numerical approach, Torrenti et al. [30] show that the mechanical percolation threshold is slightly different from the percolation threshold of solid phases because it involves not only the notion of solid skeleton continuity but also cohesion between percolated solid phases. It is thus this mechanical threshold that must be considered in the modelling of the mechanical property variations. Recently Sanahuja et al. [25], starting from previous work by Bernard et al. [6], proposed a homogenization procedure to compute this threshold. The numerical approach of Torrenti et al. [30] and the homogenization techniques are compatible and give similar values for the threshold [29]. In the following section, the threshold is assumed to be measured or computed by one of these approaches.

3.2.2 Creep properties at early age

The evolution of the elastic characteristics according to hydration development can be fitted by Eq. 19.

These laws are inspired by the Young's modulus evolution law proposed in [22, 24] cited by [13, 15] or [12].

$$k_0(\alpha) = k_{\text{th}}\left\langle\frac{\alpha-\alpha_s}{1-\alpha_s}\right\rangle^{2/3} \text{ and } \mu_0(\alpha) = \mu_{\text{th}}\left\langle\frac{\alpha-\alpha_s}{1-\alpha_s}\right\rangle^{2/3} \tag{19}$$

where: k_{th} and μ_{th} are the theoretical elastic characteristics of the completely hydrated concrete; they are the fitting parameters. α_s is the hydration degree that characterizes the percolation threshold. $\langle X\rangle$ is the positive part of X(X if $X > 0$, 0 elsewhere).

In order to limit the number of fitting parameters and for physical reasons, the evolution of the creep parameters is considered to be similar to that of the instantaneous elastic parameter (presented in Eq. 19). The medium creep parameters are thus proportional to k_0 while the deviatoric creep parameters are proportional to μ_0. The first application of the proposed model on a CEM I cement based concrete will show, through an incremental creep test at early age, that this assumption allows the tests to be fitted without any additional parameters. Moreover, proportionality between the viscosities of the short term creep module and the elastic parameters is also assumed to be as in De Shutter's works [4, 12], which implies that the characteristic time of creep is independent of the hydration degree. This second assumption was also verified experimentally as shown below.

3.2.3 Strengths at early age

The variations of the concrete compressive and tensile strengths are fitted by Eq. 20 from [20, 24] cited by [13, 15] or [12, 33].

$$Rc(\alpha) = Rc_{\text{th}}\left\langle\frac{\alpha-\alpha_s}{1-\alpha_s}\right\rangle \text{ and } Rt(\alpha) = Rt_{\text{th}}\left\langle\frac{\alpha-\alpha_s}{1-\alpha_s}\right\rangle^{2/3} \tag{20}$$

where: Rc_{th} and Rt_{th} are the theoretical strengths of the completely hydrated concrete, α_s characterizes the percolation threshold. This percolation threshold is unique because it is intrinsic to the material. It should take the same value as the one used for the elastic modulus.

4 Numerical implementation

4.1 Principle

The behaviour of hardening concrete is predicted by successively solving a multiphasic hydration model and the mechanical model presented in this article. The physicochemical phenomena due to hydration and the mechanical behaviour of concrete at early age are weakly coupled because the mechanical state does not influence hydration development (at the stress level that can be encountered in this case). The multiphasic hydration model is first solved as presented in techniques [10] and the results are used to update the mechanical characteristics and internal variables as indicated above.

The non-linear mechanical model is then solved step by step. The resolution method at each time step can be divided into nine stages:

1- The imposed mechanical strain is decomposed into a medium and a deviatoric part.
2- The creep internal variables (strains, consolidation coefficients) are recalled.
3- The mechanical characteristics are updated according to the hydration degree at the time step. (Eqs. 19, 20)
4- The strains are decomposed into elastic, viscoelastic and viscous parts and the effective stresses are evaluated by resolution and integration of the rheological system using an original method that will be presented in the next section. (Eq. 6)
5- The rheological internal variables are updated according to stress and hydration development. (Eq. 9)
6- The effective stresses are decomposed into tensile and compressive stresses.(Eq. 10)
7- The damage variables are recalled and updated according to stresses and hydration ((Eqs. 12, 13) solved by time finite difference method).
8- The apparent stresses are determined and passed to the finite element code for the nodal force calculation.
9- The apparent stresses are determined and passed to the finite element code for the nodal force calculation.

4.2 Original method for the calculation of strain increment

The set of equations modelling the creep behaviour (Eq. 6) must be integrated at each time step in order to be implemented numerically. As there is no general analytic solution, an approximate integration is proposed using the following two approximations:

- The history of the three level strains is approximated by polynomial functions of time (defined for each time step).
- A variational formulation of differential equations is built using a constant weight function. This function is integrated on the time step so as to obtain a linear system in which solutions are the coefficients of the polynomial functions used in the approximation of the strain history.

The continuity of strains and stresses between two time steps is ensured by the following five equations, in which 0^+ represents the beginning of the current time step and 0^- the end of the previous ones.

$$\begin{cases} \varepsilon_0^{(s)}(0^-) = \varepsilon_0^{(s)}(0^+) \\ \varepsilon_{KV}^{(s)}(0^-) = \varepsilon_{KV}^{(s)}(0^+) \\ \varepsilon_M^{(s)}(0^-) = \varepsilon_M^{(s)}(0^+) \end{cases} \text{and} \begin{cases} \tilde{\sigma}^{(s)}(0^-) = \tilde{\sigma}^{(s)}(0^+) \\ \tilde{\sigma}^{V(s)}(0^-) = \tilde{\sigma}^{V(s)}(0^+) \end{cases} \tag{21}$$

With the two sets of equations (Eqs. 6 and 21), eight equations are available for the determination of the polynomial functions defining the three strains (elastic, Kelvin Voigt and Maxwell levels). The Kelvin Voigt and Maxwell strains must be approximated by second order polynomial functions (parabolas with three parameters for each strain) because the viscous modules of each level introduce an acceleration term into the incremental behaviour law. This necessary choice means that the strain of the elastic level can be approximated only with a linear function (two parameters). In this development, the total strain history is imposed by the finite element code; it is actually approached by a linear function according to the values at the beginning and at the end of the time step.

Once the eight parameters are found, the strains and stresses of each level can be determined at the end of the time step.

5 Test of the model on a laboratory structure

5.1 Presentation of the structure

The model was applied to a "massive laboratory structure" in order to assess its early age cracking risk. The application chosen was the construction site of the Naga-Hammadi dam. This construction was first used to test the capability of the hydration model to predict the temperature evolution of composed binder concrete in a 27 m^3 block [10]. The aim of the study was to verify that no early age cracking would occur due to the effect of temperature development in concrete elements. As it was not technically possible to instrument the test block used in the field for the hydration validation so as to measure the strains in the block, a complementary laboratory test, representative of the thermal gradients observed on the test block, was designed. It was a massive structure at laboratory scale (60 cm diameter cylinder) made with the same binary binder as the test block in the field of the Naga Hammadi dam.

5.1.1 Material characteristics

The structure was cast with a binder composed of 60% CEM I and 40% fly ash. The concrete formulation is given in Table 1.

In order to predict the early age mechanical behaviour of the structure, the variation of the degrees of hydration of the two anhydrous phases (cement and fly ash) first had to be predicted using the multiphasic model presented in [10] (the parameters of this model are given in Table 2).

Table 1 Concrete formulation

Material	Content (kg/m^3)
Cement (CEMI 42.5N)	210
Fly ash	140
Sand 0/4 mm	763
Gravel 4/16 mm	567
Gravel 16/32 mm	574
Plasticizer	4
Effective water	131

Table 2 Parameters of the hydration model [10] for the concrete used in the laboratory structure

	Clinker	FA
Chemical parameters		
Ai	7.16×10^{7}	1.32×10^{12}
Bi	1.717	7.139
ni	0.521	0.172
ρi (kg/m^3)	3224	2200
Ri (m^3/m^3)	1.83	1.94
Qch (g/g)	0.27	−0.93
Eai/R (K^{-1})	5100	6800
Thermal parameters		
λc (J/(h m K))	6480	
cc (J/(kg K))	900	
ρc (kg/m^3)	2433	
Q_{th}^{T} (J/g)	437	570
Hydric parameters		
D_{W0} (m^2/s)	2×10^{-13}	
p (m^3/l)	0.05	
Q_{th}^{W} (g/g)	0.32	0.75

Table 3 Mechanical parameters for the concrete used in the laboratory structure

α_s	0.12
$k_{0\infty}$ (GPa)	47
$\mu_{0\infty}$ (GPa)	35
$k_{KV\infty}$ (GPa)	178.6
$\mu_{KV\infty}$ (GPa)	80.5
$\eta_{KV\infty}^{(s)}$ (GPa s)	2.44×10^{7}
$\eta_{KV\infty}^{(d)}$ (GPa s)	1.81×10^{7}
$\eta_{M\infty}^{(s)}$ (GPa s)	4.06×10^{7}
$\eta_{M\infty}^{(d)}$ (GPa s)	6.05×10^{7}
$\varepsilon_M^{(s)k}$ (m/m)	1.4×10^{-4}
$\varepsilon_M^{(d)k}$ (m/m)	8×10^{-2}
Rc_∞ (MPa)	62.6
Rt_∞ (MPa)	4.2
α^T (°C^{-1})	10^{-5}

The development of the mechanical characteristics of the concrete was then predicted, as described previously, according to the evolution of an average hydration degree. The parameter fitting of the characteristic evolution laws (Eqs. 19, 20) was performed on measurements of mechanical characteristics at several dates during the hydration. The theoretical mechanical characteristics (corresponding to an hydration degree of one) obtained are reported in Table 3, the percolation threshold is found for $\alpha = 0.12$.

Because of the physical variations of concrete in the first stages of hydration, the thermal dilatation coefficient changes rapidly during this structuring period [7]. Nevertheless, experimental results show that this coefficient quickly converges to its final value [21]. It was therefore assumed to be constant beyond the percolation threshold and equal to 10^{-5}°C^{-1}.

5.1.2 Experimental devices

The structure was first protected from heat exchanges with environment by lateral and horizontal insulation (10 cm of glass wool on the lateral face and 5 cm of expanded polystyrene on the horizontal faces). It was then placed in a temperature controlled room (Fig. 5).

For the first 20 h, the room temperature was fixed at 30°C. It was lowered to 7°C when the lateral insulation was removed. The thermal gradient between the core and the surface was thus more pronounced.

As shown in Fig. 5, the structure was equipped with thermocouples and strain gauges placed halfway up it.

5.2 Results and discussion

The hydration prediction was first validated indirectly by comparing the calculated temperature variations at the core and surface with the measurements given by the thermocouples. This comparison is presented in Fig. 6 and shows rather good concordance between model and experiments.

The strain induced by these temperature variations at early age was measured by strain gauges embedded halfway up the specimen (Fig. 5). The measurements were compared with the results obtained using the early age behaviour model implemented in the finite element code Castem [11]. Figure 7 shows quite good concordance between the experimental and model results

The model application also allowed us to study the stress and damage variation in the structure during

Fig. 5 Test procedure

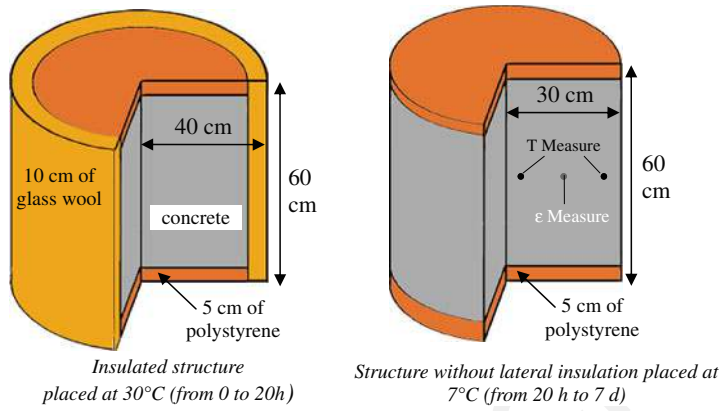

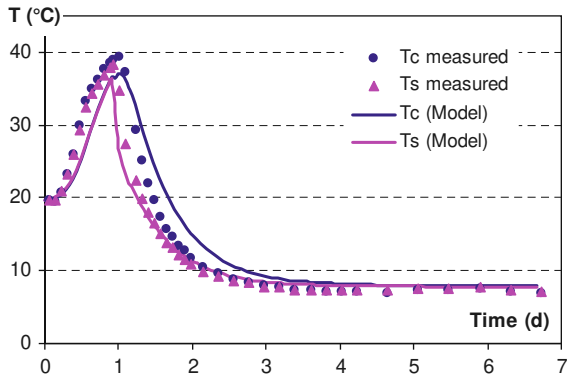

Fig. 6 Evolution of the surface temperature (T_s) and the core temperature (T_c) according to time (*full line* model results, *symbols* measurements)

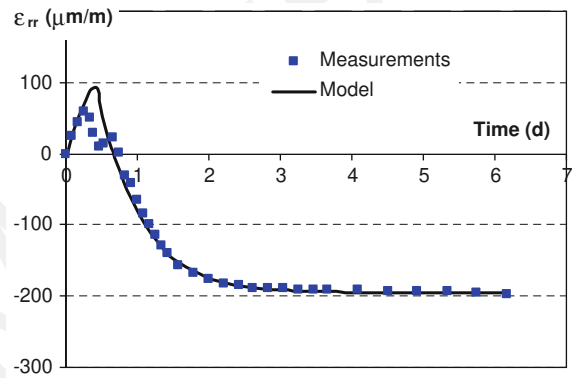

Fig. 7 Evolution of the strain halfway down the structure according to time (*full line* model results, *squares* measurements)

the test. As the formwork did not block the structure displacements, stresses were induced only by mechanical strain gradients. So, it can be seen in Fig. 8 that only weak $\sigma_{\theta\theta}$ stresses were observed before the formwork and insulation were removed (at 20 h). These weak stresses were the consequences of the low thermal gradient resulting from the small heat loss through the insulation. These stresses did not lead the structure to crack, as can be observed in Fig. 9 at 20 h (damage variable close to zero).

Once the thermal insulation and formwork had been removed, the observed thermal gradient between the core and the surface led to the development of a system of self-balanced stresses $\sigma_{\theta\theta}$ with a tensile stress on the surface due to contraction, which was strongly constrained by the core. This stress increased up to 26 h (5 h after removal of the insulation) (see Fig. 8). It induced non-localized micro-cracking on the surface because the damage variable observed in the θ direction (see Fig. 9) remained less than that associated with the peak of the tensile behaviour law (equal to 0.3 at this time, see Fig. 2). This numerical prediction was confirmed by visual observation, which did not reveal any localized cracking.

When the structure temperature became lower than the reference temperature observed at the instant of the percolation threshold (26°C), the strain on the surface became negative and led to an inversed self-balanced stress system with a compressive stress on the surface and a tensile stress at the core. This

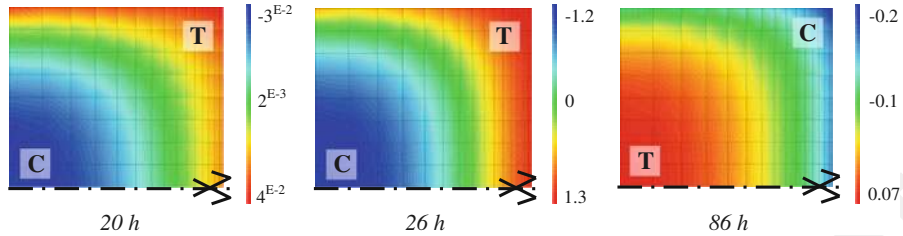

Fig. 8 Evolution of the stress $\sigma_{\theta\theta}$ on the half-structure

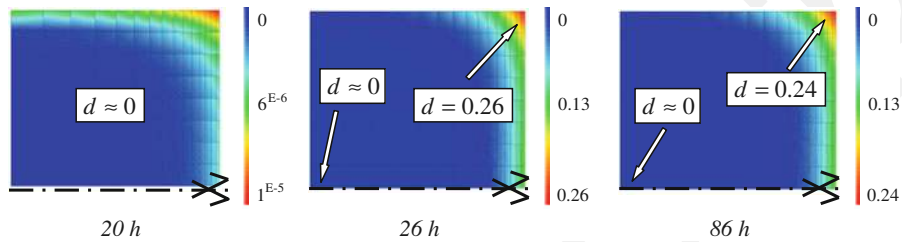

Fig. 9 Evolution of the damage variable on the half-structure (the localization occurs for damage equal to 0.3)

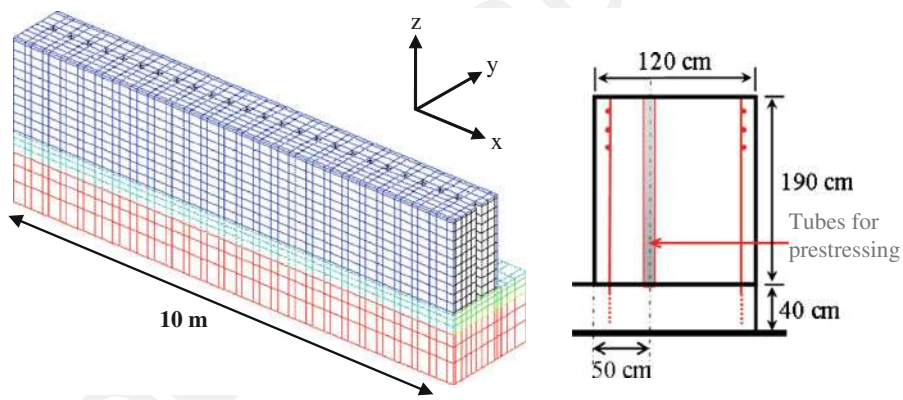

Fig. 10 Mesh and transversal section view of the Civaux wall

residual self-balanced stress system remained at very low values and decreased with time due to the stress relaxation induced by concrete creep.

6 Application to cracking risk assessment of structure in the field

6.1 Presentation of the structure

The field structure chosen for this study was a massive experimental wall built by EDF on the site of the Civaux nuclear power plant in France. The wall is 1.2 m wide, 1.9 m high and 20 m long and has a plane of symmetry at mid-length that justifies modelling only one half of the structure (Fig. 10).

The wall is reinforced by two reinforcement planes located at 5 cm from the lateral faces, and contains vertical, regularly spaced holes reserved for the prestressing cable guide tubes as presented in Fig. 10.

On the figure, it can be seen that, for hydration simulation, the bottom slab and a part of the soil were modelled as it was necessary to reproduce the thermal transfer between concrete and soil well. This transfer leads to a lower increase of temperature in the bottom of the wall than at the core.

The concrete used for this structure was designed to withstand the high stresses that can be observed in a nuclear plant. It was an HPC concrete cast with cement and silica fume (HPC formulation in Table 4). During the early age behaviour of the structure, the concrete may be subject to damage caused by the restrained thermal shrinkage induced by the heat released by the cement hydration. Therefore, EDF chose to build an experimental wall, representative of the nuclear plant walls, in order to

Table 4 Concrete formulation of the HPC wall

Material	Content (kg/m^3)
Cement CPJ 55 PM	266
Silica fume	40.3
Arlaut gravels	
12.5/25	890
4/12.5	209
0/5	873
Plasticizer (Rhéobuild)	9.08
Effective water	161 l

Table 5 Parameters of the hydration model [10] for the concrete used in the HPC wall

	Clinker	FS
Chemical parameters		
Ai	4.27×10^6	1.24×10^{18}
Bi	2.97	6.08
ni	0.260	0.483
ρi (kg/m^3)	3106	2200
Ri (m^3/m^3)	1.98	0.69
Qch (g/g)	0.31	−1.47
Eai/R (K^{-1})	4000	11600
Soil thermal parameters		
λs (J/(h m K))	2340	
ρs (kg/m^3)	2000	
cs (J/(kg.K))	800	
Concrete thermal parameters		
λc (J/(h m K))	6480	
cc (J/(kg K))	950	
ρc (kg/m^3)	2448	
Q_{th}^{T} (J/g)	454	850
Hydric parameters		
D_{W0} (m^2/s)	0.74×10^{-13}	
p (m^3/l)	0.05	
Q_{th}^{W} (g/g)	0.37	0.85

evaluate the risk of early age cracking. The fitted parameters are given in Table 5 for the hydration model [10] (convective exchanges coefficient taken equal to 19.8 kJ/h m^2 K) and in Table 6 for mechanical parameters of totally hydrated concrete (percolation threshold). The steel is considered elastic ($E_{steel} = 20.3$ GPa and $\nu_{steel} = 0.3$)

Table 6 Mechanical parameters for the concrete used in the HPC wall

$k_{0\infty}$ (GPa)	27.2
$\mu_{0\infty}$ (GPa)	16.7
$k_{KV\infty}$ (GPa)	104.2
$\mu_{KV\infty}$ (GPa)	38.9
$\eta^{(s)}_{KV\infty}$ (GPa s)	3.56×10^7
$\eta^{(d)}_{KV\infty}$ (GPa s)	2.01×10^7
$\eta^{(s)}_{M\infty}$ (GPa s)	9.00×10^7
$\eta^{(d)}_{M\infty}$ (GPa s)	7.28×10^7
$\varepsilon_M^{(s)k}$ (m/m)	2.8×10^{-5}
$\varepsilon_M^{(d)k}$ (m/m)	2×10^{-2}
Rc_∞ (MPa)	80.1
Rt_∞ (MPa)	4.13

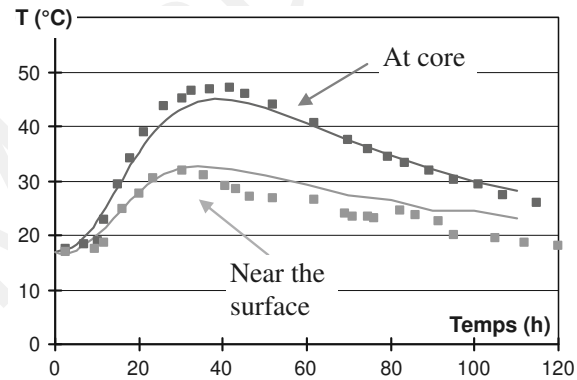

Fig. 11 Variation of temperature in the core and near the surface (*line* model, *rectangles* experiments)

6.2 Results and discussion

After the fitting of hydration parameters on a Langavant test (quasi adiabatic test), the multiphasic hydration model was applied to the structures with the mesh presented in Fig. 10 and in situ conditions (convective exchanges with the surroundings).

The temperature variations obtained at the core and near the surface are presented in Fig. 11. The model correctly reproduces the temperature in the field. It can be seen that, because of its large dimensions, the structure undergoes a large increase in temperature, mainly in the core. The surfaces experience thermal transfer by convection with the environment and have a lower temperature than the core.

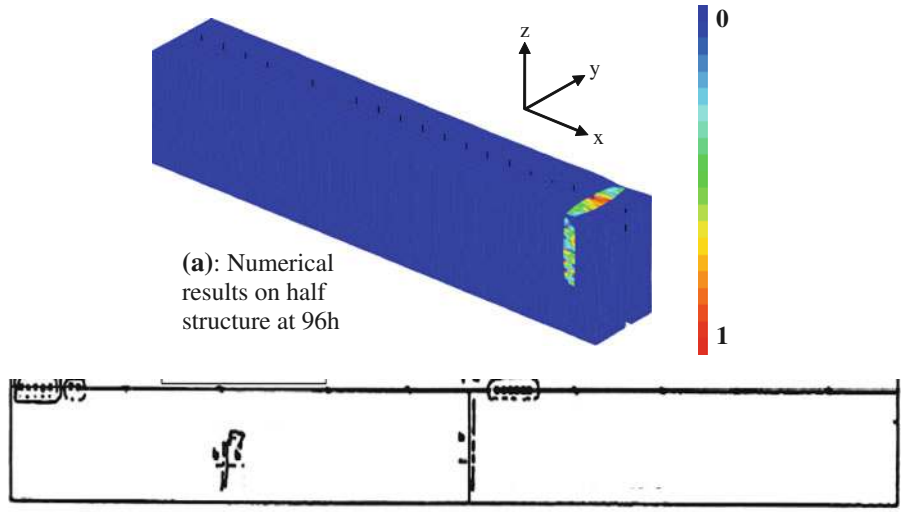

(b): Experimental observations on the entire wall

Fig. 12 Longitudinal damage field (d_{xx}) 96 h after casting and experimental observations

Table 7 Mechanical parameters for the concrete used in the HPC wall

Near the vertical reservation ($y = 63$ cm)	72.6 μm
At $y = 35$ cm	62 μm
At the reinforcement map ($y = 7$ cm)	16.3 μm

This difference between surface and core temperatures observed in Fig. 11 generates a system of self balancing stresses with tension at the surface and compression at the core. On this structure, this leads to stresses too small to produce superficial cracks just after the formwork removal.

The cracking observed on the structure 96 h after casting (see Fig. 12) was due to the global cooling of the wall that led to internal thermal contraction. As these strains were restrained by the bottom slab on the wall base, they produced tensile stresses in the entire wall, with higher values at the core (where the temperature reached its maximal value). The crack was initiated near the prestressing cable guide tubes, which constitute weak points in the structure and consequently concentrate stresses, favouring crack initiation. Fig. 12 highlights the good concordance between the model results and the observations made in situ.

In the proposed model, the crack opening can be evaluated by the discontinuity of the horizontal displacement of the node element including the localized strain corresponding to the crack. The values of crack opening for different distances to the surface are shown in Table 7. It can be noted that the crack opening is partially restrained by the reinforcement near the surface and is maximal in the core. In the field, only 1 crack was observed (Fig. 12) with a crack opening value of 100 μm. The crack openings obtained with the proposed model globally reproduce the order of magnitude but underestimate the opening value. This underestimation may be explained by the fact that the modelling of adherence between steel and concrete was not considered to be affected by hydration or damage (except indirectly by the variation of concrete tensile strength in the damage model used in the finite element surrounding the reinforcement mesh). Another explanation of this underestimation may be that the thermal dilatation coefficient was modelled as constant and equal to 10^{-5} whereas it was higher at very early age (just before the percolation threshold) and consequently led to higher thermal expansion. These observations encourage us to envision further studies on the physical phenomena occurring near the percolation threshold (fluid–solid transition of the cement paste), a period which seems to play an important role in the mechanical behaviour and the cracking risk.

7 Conclusion

This article presents simulation tools to help practitioners to choose construction processes and concrete

compositions of structures so as to control the risk of early age cracking. Using the results of a hydration model, the early age mechanical behaviour model proposed here analyses the mechanical aspects of any concrete structure subjected to the consequences of hydration (temperature rise, thermal gradients, variation in mechanical characteristics). The proposed mechanical model is based on coupling between a creep and a damage behaviour law. The creep model is based on non-linear viscoelastic incremental laws with characteristics modified by hydration development. It has been shown that the dependence of creep model parameters on hydration can be reasonably approximated by a variation law similar to those used for elastic moduli. The evolution law of the creep model parameters was firstly tested on an incremental creep test which proved its capability to reproduce the creep behaviour of a hardening concrete. The effective stresses assessed through the rheological model were then used in an anisotropic damage model. In this model, particular attention was paid to ensuring that not only the parameters but also the internal variables evolved according to the hydration. The cracking risk of a structure is thus evaluated through the evolution of the damage variable. According to the tensile behaviour law, localized cracks only appear if the damage is higher than a characteristic value corresponding to the peak of the behaviour law; when this threshold is exceeded, a strain localization controlled by a Hillerborg procedure appears, and the crack opening can then be deduced from the nodes displacement of the corresponding finite element. The model was successfully applied to validate a concrete formulation used in an actual building site and to the prediction of early age cracking of a massive reinforced structure.

Acknowledgments The authors acknowledge the financial support of the French Group *VINCI Construction Grands Projets* (associated with ANRT for the CIFRE doctoral scholarship), of the French national program CEOS.fr and the French National Research Agency (ANR) under the MEFISTO research program (control of cracking in concrete structures—grant VD08_323065). We are also grateful to *CEA/DEN/DM2S/SEMT* for providing the finite element code CASTEM2005.

References

1. Acker P, Ulm F-J (2001) Creep and shrinkage of concrete: physical origins and practical measurements. Nucl Eng Des 203:143–158
2. Bažant ZP, Prasannan S (1989) Solidification theory for concrete creep I. Formulation. J Eng Mech 115(8):1691–1703
3. Benboudjema F, Torrenti J-M (2006) Early age behaviour of concrete nuclear containments. In: 2nd edition of the international symposium on advances in concrete through science and engineering, RILEM Publication PRO 51, Quebec
4. Benboudjema F, Torrenti JM (2008) Early age behaviour of concrete nuclear containments. Nucl Eng Des 238(10): 2495–2506
5. Bentz DP (2000) CEMHYD3D: a three-dimensional cement hydration and microstructure development modelling package. Version 2.0. NISTIR 6485, U.S. Department of Commerce, Washington, April 2000
6. Bernard O, Ulm F-J, Lemarchand E (2003) A multiscale micromechanics-hydration model fir the early age elastic properties of cement-based materials. Cem Concr Res 33: 1293–1309
7. Bjøntegaard Ø, Sellevold EJ (1998) Thermal dilatation—autogenous shrinkage: how to separate? In: Autogenous shrinkage of concrete: proceedings of the international workshop of Hiroshima, Hiroshima, Japan, June 1998
8. Brooks JJ (2005) 30-Year creep and shrinkage of concrete. Mag Concr Res 57(9):545–556
9. Buffo-Lacarrière L, Sellier A (2009) Behaviour of HPC nuclear waste storage structures in leaching environment. In: Concrete in aggressive aqueous environments, RILEM TC 211-PAE final conference, Toulouse, France, 3–5 June 2009
10. Buffo-Lacarrière L, Sellier A, Escadeillas G, Turatsinze A (2007) Multiphasic finite element modelling of concrete hydration. Cem Concr Res 37(2):131–138
11. Cast3M (2005) CEA—DEN/DM2S/SEMT. http://www-cast3m.cea.fr/cast3m/index.jsp
12. De Schutter G (2002) Finite element simulation of thermal cracking in massive hardening concrete elements using degree of hydration based material laws. Comput Struct 80:2035–2042
13. Eierle B, Schikora K (1999) Computational modelling of concrete at early ages using DIANA. In: Diana-World 1999, issue 2. http://www.bst.bv.tum.de/pdf/diana.pdf
14. François D, Pineau A, Zaoui A (1991) Comportement mécanique des matériaux, vol 1. Hermès, Paris, ISSN 0986-4873
15. Gutsch A, Rostásy FS (1994) Young concrete under high tensile stresses—creep, relaxation and cracking. In: Thermal cracking at early ages, Rilem proceeding 25. Munich, Deutschland, ISBN 0-419-187103, pp. 111–119
16. Hauggaard AB, Damkilde L, Hansen PF (1999) Transitional thermal creep of early age concrete. J Eng Mech 125(4):458–465
17. Hillerborg A, Modeer M, Petersson PE (1976) Analysis of crack formation and crack growth in concrete by means of fracture mechanics and finite elements. Cem Concr Res 6:773–782
18. Ishikawa Y, Kunieda M, Srisoros W, Tanabe T (2005) Constitutive law based on solidification. In: Creep, shrinkage and durability of concrete and concrete structures (CONCREEP 7), Ecole Centrale de Nantes, Nantes, 12–14 September 2005
19. Kachanov LM (1986) Introduction to continuum damage mechanics. Martinus Nijhoff, Dordrecht. ISBN 90-247-3319-7

20. Lackner R, Mang HA (2004) Chemoplastic material model for the simulation of early-age cracking: from the constitutive law to numerical analyses of massive concrete structures. Cem Concr Compos 26:551–562
21. Laplante P, Boulay C (1994) Evolution du coefficient de dilatation thermique du béton en fonction de sa maturité aux tout premiers ages. Mater Struct 27:596–605 (in French)
22. Laube M (1990) Werkstoffmodell zur Berechnung von Temperaturspannungen in massigen Betonbauteilen im jungen Alter. Dissertation TU Braunschweig
23. Mabrouk R, Ishida T, Maekawa K (2004) A unified solidification model of hardening concrete composite for predicting the young age behavior of concrete. Cem Concr Compos 26:453–461
24. Onken P, Rostásy F (1995) Wirksame Betonzugfestigkeit im Bauwerk bei früh einsetzendem Temperaturzwang. DAfStb Heft 449. Beuth-Verlag, Berlin
25. Sanahuja J, Dormieux L, Chanvillard G (2007) Modelling elasticity of a hydrating cement paste. Cem Concr Res 37:1427–1439
26. Sellier A, Bary B (2002) Coupled damage tensors and weakest link theory for the description of crack induced anisotropy in concrete. Eng Fract Mech 69:1925–1939
27. Sellier A, Buffo-Lacarriere L (2009) Toward a simple and unified modelling of basic creep, shrinkage and drying creep for concrete. Eur J Environ Civil Eng 13(10):1161–1182
28. Smilauer V, Bittnar Z (2006) Microstructure-based micromechanical prediction of elastic properties in hydrating cement paste. Cem Concr Res 36(9):1708–1718
29. Stefan L, Benboudjema F, Torrenti J-M, Bissonnette B (2010) Prediction of elastic properties of cement pastes at early ages. Comput Mater Sci 47(3):775–784
30. Torrenti J-M, Bendoudjema F (2005) Mechanical threshold of cementitious materials at early age. Mater Struct 38(277):299–304
31. Ulm F-J, Coussy O (1998) Couplings in early-age concrete: from material modeling to structural design. Int J Solids Struct 35(31–32):4295–4311
32. Van Breugel K (1995) Numerical simulation of hydration and microstructural development in hardening cement-based materials. Cem Concr Res 25(2):319–331
33. Waller V, D'Aloïa L, Cussigh F, Lecrux S (2004) Using the maturity method in concrete cracking control at early ages. Cem Concr Compos 26:589–599
34. Yang Q-S, Li C-J (2006) Evolution of properties in hydration of cements: a numerical study. Mech Res Commun 33:717–727